

Contents lists available at ScienceDirect

Soil Dynamics and Earthquake Engineering

journal homepage: www.elsevier.com/locate/soildyn





A numerical approach for simulation of stress-controlled cyclic shear loading in a soil column considering partial drainage

Waleed El-Sekelly ^{a,b,*}, Ricardo Dobry ^c, Tarek Abdoun ^{b,c}

- a Dept. of Structural Eng., Mansoura University, Mansoura, 35516, Egypt
- ^b New York University Abu Dhabi, P.O.Box 129188 Abu Dhabi, United Arab Emirates
- ^c Dept. of Civil and Environmental Eng., Rensselaer Polytechnic Institute, Troy, NY, 12180, USA

ARTICLE INFO

Keywords: Sand liquefaction Undrained Partial drainage Constitutive modeling

ABSTRACT

Liquefaction strength curves (LSCs) are commonly generated based on undrained stress-controlled cyclic testing to define the liquefaction potential of sands. However, these LSCs do not consider the effect of partial drainage on liquefaction potential. This is mainly because there are very limited experimental techniques to run stresscontrolled tests for partially drained sands. This manuscript proposes a procedure to numerically simulate a saturated sand column with a free drainage boundary at the top (or top and bottom), accelerated horizontally at the bottom with constant acceleration cycles of duration designed to generate constant cyclic shear stress histories in the column. This is done for columns subjected to low and high overburden pressures. The paper starts with numerical simulations of a typical undrained cyclic direct simple shear, CDSS tests by applying a stepped velocity wave to a single soil element, an already established approach. This approach only works for a single element in undrained condition which is fixed at the base. Then, the proposed procedure is implemented by applying stepped acceleration time histories at the base of soil columns having one or two drainage boundaries. In these stepped acceleration runs, the durations of the acceleration cycles are controlled to achieve a partially drained stress-controlled CDSS kind-of-loading at specific elevations within the soil columns. The technique is used to show the effect of partial drainage on sand liquefaction behavior at both low and high overburden pressures. The results show that the effect of drainage is much more significant at higher overburden. The existence of both top and bottom drainage boundaries resulted in less liquefaction vulnerability, as compared to having only one drainage boundary at the top of the sand column. The results show that liquefiable sand layers in the field may be less prone to liquefaction under high overburden pressure than predicted by the current state-ofpractice, which relies mainly on undrained small-scale cyclic tests.

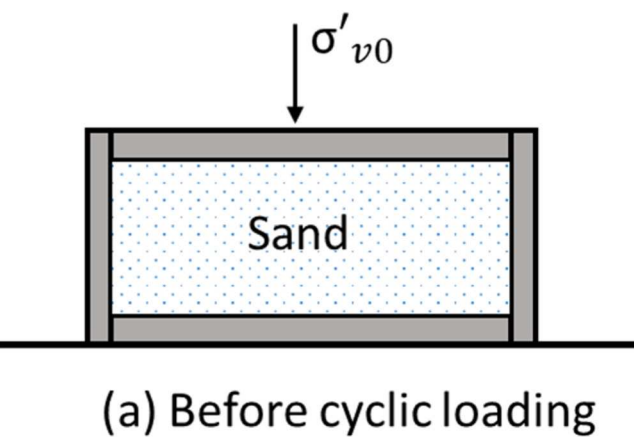
1. Introduction

Earthquake-induced sand liquefaction has been a concern in the last several decades due to its severe consequences. Structures founded on soils that liquefy often suffer severe damage during and after earthquakes. Practical liquefaction applications depend on defining the Cyclic Stress Ratio (CSR) - quantifying the earthquake demand - and the Cyclic Resistance Ratio (CRR) – representing the site resistance. In the typical deterministic approach, liquefaction is predicted if CSR is greater than CRR. This procedure is called the Simplified Approach [1]. The CRR is either evaluated from a field test (Standard Penetration Test, SPT, Cone Penetration Test, CPT, or shear wave velocity, Vs). Alternatively, the CRR can be obtained from small-scale undrained cyclic loading lab

experiments (cyclic triaxial, CTX; or cyclic direct simple shear, CDSS). The CDSS test is sketched in Fig. 1. It has the advantage over the CTX test that the CDSS generates a similar stress path to that associated with the actual ground shaking in the field.

Field experiments are used to determine the CRR in most practical applications. On the other hand, the lab-determined CRR is commonly used to: (i) calibrate constitutive models; and (ii) determine correction factors to be used together with the field liquefaction triggering charts developed as part of the Simplified Procedure. Specifically, undrained cyclic lab tests have been used to determine the correction factors for overburden pressure K_{σ} and for static shear stresses, K_{α} [2]. The use of factors K_{σ} and K_{α} is necessary in some practical situations, because practical field liquefaction charts are typically calibrated and

^{*} Corresponding author. Dept. of Structural Eng., Mansoura University, Mansoura, 35516, Egypt. *E-mail address:* welsekelly@mans.edu.eg (W. El-Sekelly).



(a) Before cyclic loading $\sigma'_{v} = \sigma'_{v0} - u$ $\uparrow^{\tau_{c}}$ Sand

(b) During cyclic loading

Fig. 1. Sketch of Cyclic Direct Simple Shear (CDSS) apparatus.

normalized using liquefaction case histories subjected to initial vertical effective pressures in the order of 100 kPa (\sim 1 atm) and small or no initial driving static shear stresses.

Small-scale lab tests on saturated sand such as that shown in Fig. 1, are often performed undrained to generate the liquefaction strength curves (LSCs), such as those shown in Fig. 2 from De Alba et al. [3] for different relative densities. Each data point in the figure represents the number of cycles (N) of a certain cyclic stress ratio, CSR, required to cause liquefaction (CSR = cyclic shear stress/initial effective vertical stress = τ_c/σ'_{v0}). While CSR can be defined for any N, CRR=CSR associated with a specific N, typically N = 5, 10 or 15 cycles, depending on

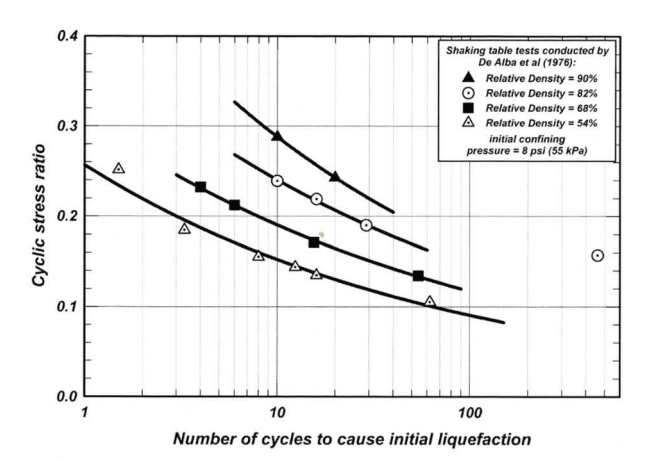


Fig. 2. Cyclic stress ratio (CSR) versus number of cycles (N) required to reach liquefaction defined by excess pore pressure ratio, $r_u=100$) (liquefaction strength curves, LSC) for CDSS tests by De Alba et al. [3] (reported by Ref. [2]).

the duration of the design earthquake.

Vaid and Sivathayalan [4] studied the effect of relative density, $D_{\rm r}$, and confining pressure on the CRR of Fraser Delta sand for N = 10 cycles, see Fig. 3a. While Fig. 3a was obtained from CTX tests, the trends for CDSS tests are the same. Fig. 3a shows that CRR increases with increased $D_{\rm r}$, as expected. It also shows that CRR decreases with increasing confining pressure. This last effect is more significant at a higher $D_{\rm r}$.

The ratio between CRR at any overburden pressure $(\sigma'_{\nu 0})$ and CRR at $\sigma'_{\nu 0}=100$ kPa ($\sim\!1$ atm) was defined by Seed [5] as the stress correction factor, $K_{\sigma}=(CRR)_{\sigma'\nu 0}/(CRR)_1.$ Several researchers have studied K_{σ} in the laboratory and have invariably obtained a $K_{\sigma}<1.0$ for $\sigma'_{\nu 0}>1$ atm [2, 6–14]. All this research has been based on experimental or analytical frameworks related to undrained cyclic testing. During undrained cyclic loading of loose-of-critical sands, the sand skeleton tries to contract due to its tendency to densify. As a result of the enforced constant volume and constant total stress conditions, the initial normal stress $\sigma'_{\nu 0}$ is transferred cycle after cycle from the sand skeleton to the pore water, with the effective stress, σ'_{ν} decreasing and the pore pressure, u increasing. The mechanism of undrained loading is explained in Fig. 4 during one cycle of loading, as follows.

- The dynamic loading causes contraction of the sand skeleton which, if drained, would have resulted in plastic volumetric strain measured by the void ratio in the plot - moving the point from A to B in Fig. 4.
- During undrained loading, this plastic volumetric strain is compensated by elastic rebound of the skeleton due to the reduced effective stress; moving from point B to point C. The horizontal distance between points B and C measured the increase in pore pressure, Δu .
- While in the completely undrained situation, the elastic rebound in Fig. 4 moves the state of the soil from point B to point C, partial drainage behavior would stop the process at intermediate point P. The degree of partial drainage determines how close the point P is either to point B (fully drained) or to point C (fully undrained).

Some recent liquefaction research has shown that in several field situations, liquefaction is not fully undrained but rather a partially drained process [15-22]. Ohara and Yamamoto [15] carried out a series of shaking table tests, controlling the drainage boundary condition through a valve to investigate the drainage effect on liquefaction. Later, Yamamoto et al. [17] devised a test scheme involving cyclic triaxial tests simulating the drainage boundary condition under seismic loading using a triaxial apparatus equipped with a valve to accurately measure water squeezed out. Their findings demonstrated that soil samples subjected to partial drained conditions exhibited superior resistance to liquefaction compared to those under undrained conditions. Similar findings were also concluded by Adamidis and Madabhushi [19] based on dynamic centrifuge experiments. Chen et al. [20] conducted a series of cyclic triaxial tests on granular fill material under partially drained conditions. They found that the granular fill exhibited an initial significant decrease in stiffness and rapid deformation during the early cycles of loading, followed by a gradual reduction in excess pore water pressure generated. Most Recently, Abdoun et al. [21] and Ni et al. [22] conducted a systematic centrifuge experimental program studying clean sand liquefaction under high and low vertical effective stresses. They found that partial drainage increased significantly at a high vertical effective stresses, with corresponding decrease in liquefaction potential.

The findings by Abdoun et al. [21] mean that liquefaction strength curves such as those of Fig. 2 may not be representative of field situations significantly influenced by partial drainage. A possible option is to generate similar curves modified for partial drainage, with the degree of drainage and location of the curve customized to the actual drainage condition of the field situation being considered. While this kind of test and partially drained liquefaction curve generation is hard to accomplish experimentally, it is possible to achieve numerically.

This paper uses an established numerical platform to run numerical

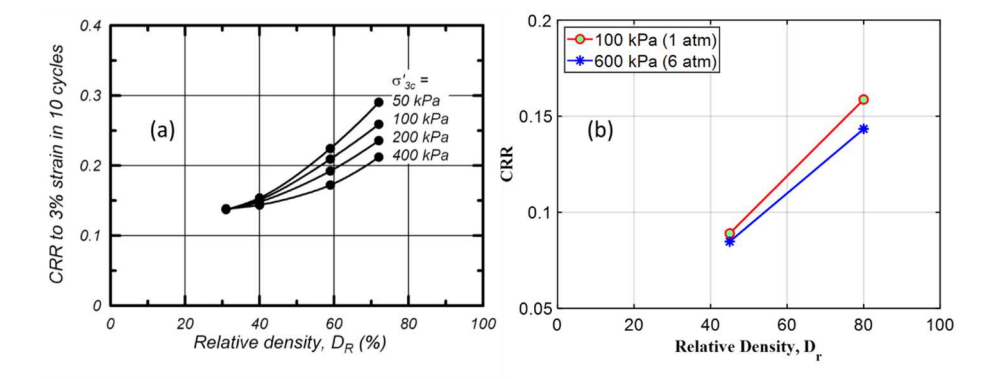


Fig. 3. (a) CTX test results for clean Fraser Delta sand, showing the CRR in 10 uniform cycles at D_r values of 31–72% and effective consolidation stresses of 50–400 kPa [2], and (b) CDSS numerical simulation (using P2Psand constitutive model and FLAC3D platform) of Ottawa F65 sand showing the CRR in 10 uniform cycles at D_r values of 45–80% and effective consolidation stresses of 100 and 600 kPa.

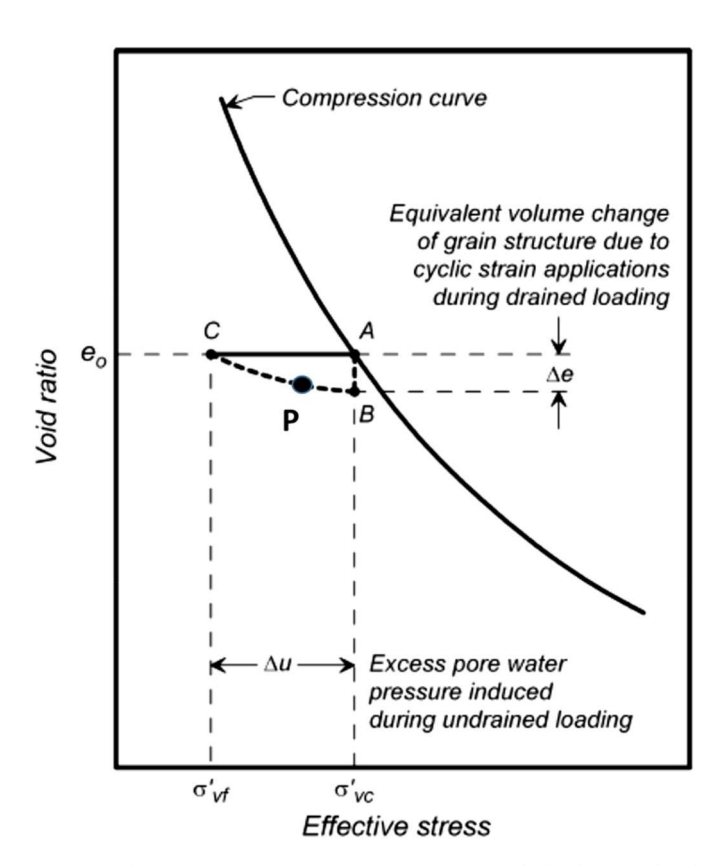


Fig. 4. Mechanism of pore pressure generation during cyclic loading (Modified after Idriss and Boulanger [2]).

stress-controlled cyclic experiments both in undrained as well as partially drained conditions. While the work presented herein only covers some limited cases of partial drainage, it paves the road for researchers and practitioners that may want to use this tool in future applications. The following section explains the scope of the paper along with the proposed methodology. The rest of the paper explains the numerical platform and the constitutive model used as well as the simulation results.

2. Scope

The purpose of the paper is to develop and validate an approach to perform numerical stress-controlled cyclic experiments under undrained as well as partially drained conditions. The numerical work is performed

in FLAC3D platform (Fast Lagrangian Analysis of Continua in 3 Dimensions). The constitutive model used in the numerical simulation is the P2Psand (Practical Two-surface Plastic Sand). P2Psand was developed and implemented in FLAC3D by Cheng and Detournay [23], based on the bounding surface model originally developed by Dafalias and Manzari [24]. The authors calibrated and validated the use of P2Psand in El-Sekelly et al. [25], where they performed a unified calibration scheme for Ottawa F65 clean sand based on stress controlled CTX, as well as centrifuge experiments under high and low confining pressures. As a final result, they generated a unified set of parameters to be used for a wide range of confining pressures. The calibration performed by El-Sekelly et al. [25] is used as the cornerstone for the simulations performed herein. The rest of the paper starts with a brief description of the numerical model and platform used in the analysis. This set of numerical model and platform is then implemented to model undrained stress-controlled CDSS tests. Following that, a brief description of two centrifuge tests is presented along with their corresponding numerical simulations using the same platform and model. Finally, the proposed numerical approach is explained and utilized to perform partially drained stress controlled cyclic tests in soil columns. This technique is used to show the effect of drainage boundaries on the liquefaction behavior at low and high overburden pressures.

3. Numerical platform and constitutive model

FLAC3D was used in all simulations presented herein. FLAC3D uses an explicit finite volume formulation in an explicit, Lagrangian calculation scheme and the mixed-discretization zoning technique. Engineering practitioners often use FLAC3D in analysis of soil and soil-structure interaction problems. Herein, FLAC3D is used in dynamic liquefaction evaluation and thus the dynamic analysis feature was activated in the code. All numerical simulations were performed in the time domain. The simulations were fully coupled, non-linear and path-dependent computations. In FLAC3D, the elements are defined as zones connected together with grid points.

The numerical analyses presented herein were performed using the P2Psand constitutive model. This model was developed by Cheng and Detournay [23] following critical state soil mechanics formulations. P2Psand is a modification of the DM04 model [24], as it maintains the original bounding surface framework with some improvement in the performance and complexity of DM04. Cheng and Detournay [23] used relative density rather than void ratio to define the state parameter. The following subsection summarize the elastic as well as the critical state formulations. Detailed model formulations can be found in Cheng and Detournay [23].

3.1. P2Psand model formulation

• Elastic formulations

The hypoelastic formulation is adopted in the elasticity phase with the following incremental form:

$$\Delta p = -K\Delta \varepsilon_{v}^{e}, \Delta s_{ij} = 2G\Delta \varepsilon_{ij} \tag{1}$$

$$p = -tr(\boldsymbol{\sigma})/3 \tag{2}$$

$$s = \sigma + pI \tag{3}$$

$$\boldsymbol{\varepsilon} = \boldsymbol{\varepsilon} - (\varepsilon_{v} / 3) \boldsymbol{I} \tag{4}$$

where p is mean pressure defined, s is deviatoric stress tensor, I is unit tensor, ε_v is volumetric strain, and ε is deviatoric strain tensor.

$$G = G_r p_{atm} \left(\frac{p}{p_{atm}}\right)^{0.5}, K = \frac{2(1+v)}{3(1-2v)}G$$
 (5)

where K and G are elastic shear and bulk modulus, respectively, ν is Poisson's ratio, and p_{atm} is reference atmospheric pressure.

• Critical State formulation

The critical state curve follows the following formulation with the state parameter as a function of relative density, D_r , rather than void ratio, e

$$D_{rc} = \frac{R}{Q - \ln\left(\frac{100p_c}{p_{am}}\right)} \tag{6}$$

where R and Q are the critical state parameters.

El-Sekelly et al. [25] showed that P2PSand can be used for a wide range of initial relative densities and initial stress states with the same general model parameters. Table 1 and the following subsection summarize the main calibration parameters in P2Psand. Details of the model calibration and comparison between experimental and numerical behavior can be found in El-Sekelly et al. [25].

3.2. Main calibration parameters

Table 1 lists the parameters used in P2Psand model, as calibrated by El-Sekelly et al. [25]. They calibrated P2Psand in four main steps: (i) initial calibration using available stress controlled CTX results on dense

Table 1P2Psand parameters used in FLAC3D simulations.

Parameter	$Dr\approx 45\%$	$Dr\approx 80\%$	
factor-cyclic K _c	0.8	0.32	
pressure-reference	101.3 kPa		
friction-critical φ_{cs}	33°		
coefficient-bounding n^b	0.0775		
coefficient-dilatancy n^d	1		
critical state parameter Q	9		
critical state parameter R	1		
dilatancy-ratio-minimum K_{LB}^d	0.7	,	
elasticity-r G _r	596	772	
fabric-maximum, z_{max}	15		
factor-degradation k_d	0.3	0.19	
Poisson's ratio v	0.1		
rate-fabric, c_z	596	772	
rate-plastic-shear h_0	0.4	ŀ	
rate-plastic-volumetric A_{d0}	Estimated Internally		
ratio-reverse	0.02		
ratio-strength, c	0.69		
void-maximum e_{max}	0.78		
void-minimum e _{min}	0.5	1	

soil of the same clean Ottawa F65 sand performed in Liquefaction Experiment and Analysis Projects, LEAP [26]; (ii) comparison between FLAC3D predictions using this calibration, and the response measured in the centrifuge tests on dense sand; (iii) adjustment of the calibration to refine the parameters controlling fluid dissipation, which is a characteristic not captured by the undrained CTX tests; and (iv) estimating the rate of cyclic mobility (i.e. contraction parameter) for loose sand using CTX results as well as centrifuge experiments (see Ref. [25] for more details). This calibration procedure yielded a very good match between the experimental and numerical simulations both at the element level as well as the system level, as shown by El-Sekelly [25]. Based on that calibration, eight main parameters were changed from their default values. Three of those eight parameters depend on the initial relative density of the deposit. These three parameters are.

- ullet The "relative-density-initial, D_r^0 " which defines the initial relative density of the sand.
- The "factor-cyclic, K_c " which defines the rate of cyclic mobility and liquefaction.
- The "elasticity-r, G_r " which defines the modulus of elasticity of the sand deposit.

The other five parameters changed from the default values are independent from the relative density or any other initial conditions, i.e. they remain unchanged for the same type of sand. These parameters are.

- The "coefficient-dilatancy n^{d} ", which defines the dilation surface.
- The "critical state parameter Q", which defines the critical state curve in the e-p' space.
- The "Poisson Ratio v", which defines the fluid diffusivity in sand by defining the elastic bulk modulus, K from the given elastic shear modulus, G.
- The "rate-plastic-shear h₀", which defines the plastic modulus from the given elastic shear modulus, G.
- The maximum and minimum void ratios "emax and emin"

Two types of simulations were used in this research. The first is a simulation of the usual *undrained* stress-controlled CDSS tests. The second type is a simulation of a *partially drained* stress-controlled cyclic tests associated with some possible field drainage scenarios.

The next section utilizes the P2Ps and model previously calibrated by El-Sekelly et al. [25] to simulate a single element undrained CDSS using FLAC3D platform.

4. Single element undrained CDSS simulations

The following are the features of the undrained simulations.

- One 8-nodes brick zone was used to simulate a small-scale lab CDSS test. Only one zone was needed since the stress state in the sample is about constant due to the small sample size.
- No drainage was allowed at any of the four sample boundaries.
- The mechanical boundary conditions were fixed at the base and free elsewhere.
- A stepped velocity function was applied at the top boundary, consisting of a constant velocity that reverses direction once the shear stress reaches a predefined level.

This same approach has been successfully used by several numerical modelers over the years using multiple models and platforms. It was lately explained and implemented by Montgomery and Ziotopoulou [27] in their simulation for the LEAP, using the PM4sand constitutive model and the FLAC platform.

The simulation results are summarized in Figs. 5–7 and Fig. 3b. Fig. 5a and b shows the liquefaction strength curves (LSC) for

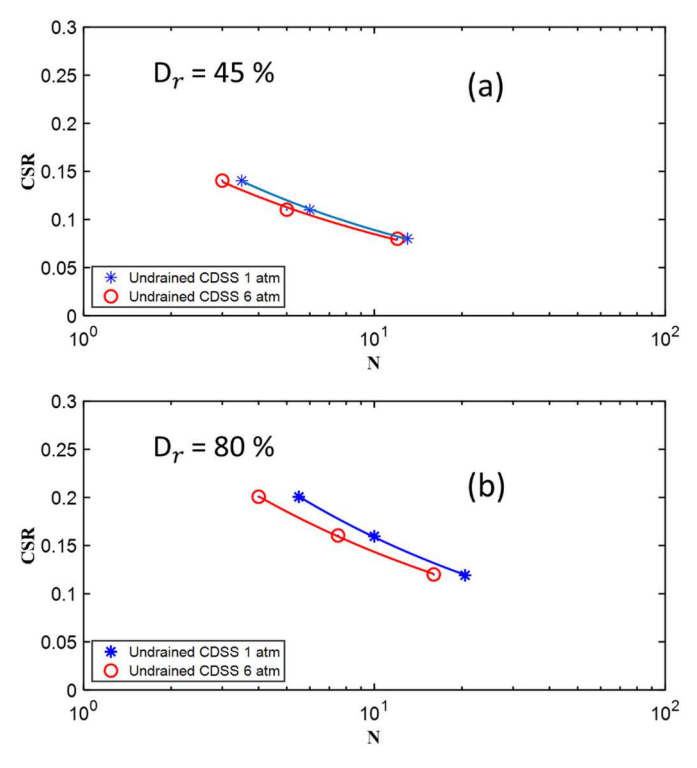


Fig. 5. LSCs from FLAC3D numerical simulations of undrained CDSS single element tests, using P2Psand model for: a) $D_r = 45\%$, b) $D_r = 80\%$.

numerical undrained CDSS tests at $D_r=45\%$ and 80%, respectively. The figures include the liquefaction strength curves at 100 (\sim 1 atm) and 600 kPa (\sim 6 atm), representing relatively low and high confining stresses, respectively. It can be noted from the figure that.

- \bullet The LSCs for $D_r=80\%$ are significantly higher than that for $D_r=45\%$, both at 1 and 6 atm. This indicates a lower liquefaction vulnerability at higher D_r , as expected.
- The LSC moves downwards as the confining stresses increases. This is consistent with the relevant undrained results of this type in the literature, for which liquefaction resistance invariably decreases as the confining pressure increases. In other words, the value of K_{σ} goes lower as the confining pressure goes higher, with all state-of-practice proposed K_{σ} curves sharing this basic feature [2,9].
- For the same D_r , the LSCs are generally parallel to each other indicating little effect of number of cycles on the ratio between the curves. In other words, in first approximation K_σ may be assumed to be independent on the number of cycles for undrained loading.
- \bullet The effect of confining pressure on the LSC is more significant at $D_r = 80\%$ compared to 45%.
- Fig. 3a -already discussed-shows the CRR for N = 10 cycles measured experimentally in CTX tests by Vaid and Sivathayalan [4] on Fraser Delta sand at different confining pressures and reported by Idriss and Boulanger [2]. Fig. 3b shows the similar CRR for N = 10 cycles computed numerically in the CDSS simulations presented herein. Both the experimental and numerical simulations show similar trends of increased CRR with increased D_r, and of decreased CRR with increased confining stress, with this last effect being more significant at a higher D_r.

Fig. 6 shows, respectively from top to bottom, the shear stress ratio-strain loops, stress path (shear stress ratio versus effective stress), excess pore pressure versus shear strain, and excess pore pressure time histories for $D_r = 45\%$ at 1 and 6 atm at a similar CSR. The figure shows the effect of confining pressure on the dilative behavior of the sand. This may be noticed from the loop reversal of the last cycle in the stress path, which

shows higher dilative response at 1 atm (100 kPa) as compared to 6 atm (600 kPa). This dilative behavior may also be observed from the "shark fin" shape of the shear stress ratio-strain loops as well as the dip in $r_{\rm u}$ at the end of shaking. All these aspects are consistent with the available experimental evidence, showing that the dilative response increases as the confining pressure decreases [2]. Fig. 7 shows a similar behavior for Dr = 80%. By comparing Figs. 6 and 7, it may be noted that the dilative response is more significant at Dr = 80%, again fully consistent with the experimental and analytical evidence reported by Idriss and Boulanger [2].

5. Numerical simulation of centrifuge experiments

Two centrifuge experiments were performed by Ni et al. [22] on clean Ottawa sand with relative density, Dr = 45%, in order to inspect the liquefaction behavior of sand in idealized field conditions under low and high overburden pressures. The two experiments were conducted under overburden pressures of about 100 kPa (Test 45-1) and 600 kPa (Test 45-6) acting on the middle of the sand layer (Table 2). The centrifuge tests were performed at the Rensselaer Polytechnic Institute (RPI) centrifuge facility using the lightweight aluminum laminar container, which has the flexible walls needed to deform horizontally simulating the desired shear beam field behavior. The soil models simulate a 5 m saturated sand layer in prototype scale, located at shallow and deep elevations under the ground surface. The sand layer was overlain by a dry layer of heavy lead grains used to achieve the required effective overburden pressure, as well as the horizontal inertia forces acting on the sand layer during shaking due to the overlying soil in the field. A thin transition layer of coarse sand and gravel was placed between the saturated sand layer and the lead grains to act as a filter to avoid sinking of lead grains into clean sand. Viscous fluid with appropriate viscosity was used in sand saturation instead of water, in order to ensure appropriate fluid flow behavior based on the centrifuge g-level of each experiment. The sand saturation followed the standard procedure adopted at RPI to ensure full saturation of the layer. The soil model was instrumented with accelerometers and pore pressure transducers, in addition to other sensors. Fig. 8 shows the model layout and instrumentation setup. The soil model was subjected to horizontal base acceleration and the soil response was recorded at different locations in the model. Fig. 9a and b shows the input acceleration, shear stress ratio (shear stress/initial vertical effective stress), and r_u ($r_u = excess\ pore$ pressure/vertical effective stress = u/σ'_{v0}) in the sand at the bottom of Tests 45-1 and 45-6, where the maximum ru values occurred. Additional details about the centrifuge tests can be found in Ni et al. [22].

El-Sekelly et al. [25] numerically simulated these centrifuge Tests 45-1 and 45-6 using FLAC3D and the P2Psand model (labelled Flac 45-1 and Flac 45-6 simulations, respectively). The model description and calibration were briefly explained in a previous section herein. More details can be found in El-Sekelly et al. [25]. The numerical work simulated a soil column in prototype scale in the centrifuge soil model. The model was built using 8-nodes brick zones stacked on top of each other and connected at the nodes. All nodes at the same elevation were linked to move together simulating the shear beam behavior modeled in the centrifuge model using the laminar container. First, the initial geostatic conditions were established using the Mohr Coulomb soil model, where the base was fixed, and the sides were allowed to only move vertically. After that, the dynamic phase of the analysis started with the sand being assigned the P2Psand model, and the sides were allowed to move freely. Then, the centrifuge base horizontal motion was applied at the bottom of the soil column. The numerical hydraulic boundary conditions simulated that of the centrifuge tests; impervious sides and base and pervious at the top of the layer. The numerical simulation was a fully coupled effective stress simulation, allowing for pore pressure generation, dissipation and redistribution. Additional details about the numerical simulation are presented by El-Sekelly et al. [25].

Fig. 9a and b shows the base acceleration, shear stress ratio and

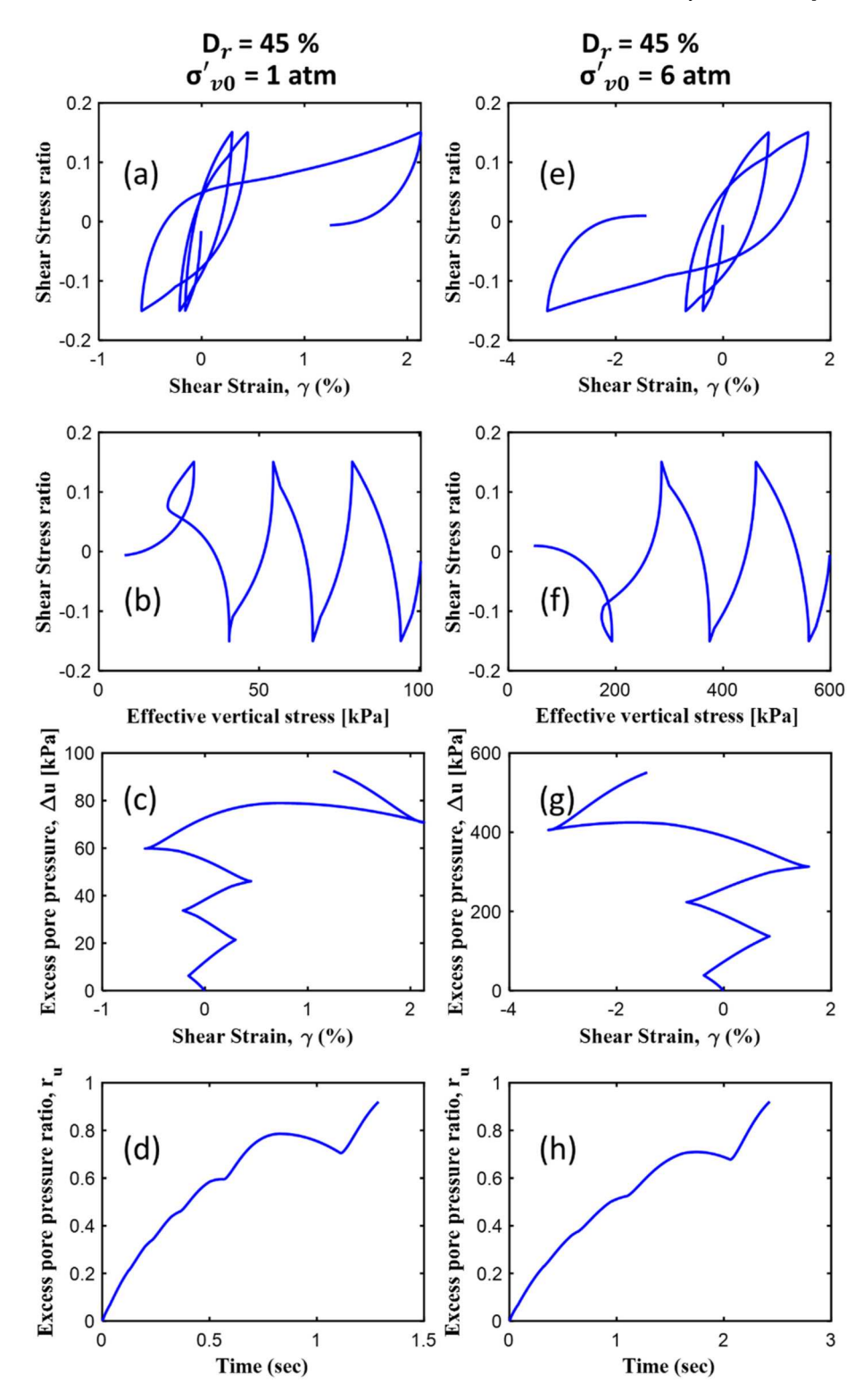


Fig. 6. Shear stress ratio-shear strain loops, stress path, shear strain versus excess pore pressure, and excess pore pressure ratio time history for Dr = 45% at (a–d) initial effective confining pressure, $\sigma_0 = 100$ kPa (~ 1 atm), and (e–h) initial effective confining pressure, $\sigma_0 = 600$ kPa (~ 6 atm).

excess pore pressure ratio computed close to the base in simulations Flac 45-1 and Flac 45-6, respectively, along with the corresponding experimental results. The numerical input accelerations used in Flac 45-1 and Flac 45-6 were the same experimentally recorded in centrifuge Tests 45-1 and 45-6, respectively.

Fig. 9a and b shows a very good match between experimental and simulated shear stress ratio records. The experimental shear stress ratio

was computed using the System Identification technique [22,28,29]. The shear stress ratios cycles have mostly similar amplitudes in the first few cycles but then starts to degrade as the excess pore pressure increases.

Fig. 9a and b also show that the computed excess pore pressure ratio buildups match very well the experimental records at both 1 and 6 atm. Abdoun et al. [21] showed that the pore pressure dissipation after the

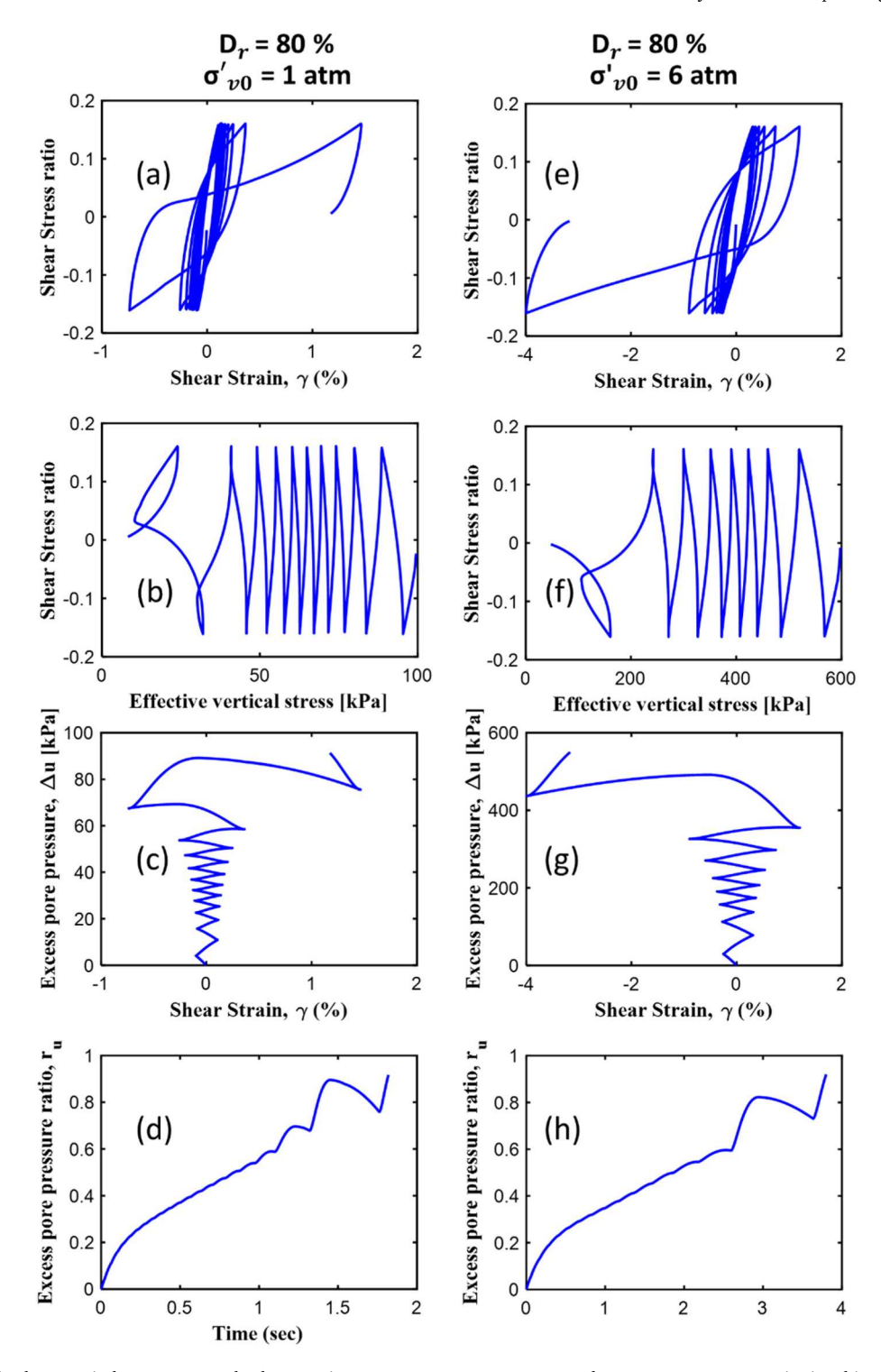


Fig. 7. Shear stress ratio-shear strain loops, stress path, shear strain versus excess pore pressure, and excess pore pressure ratio time history for Dr = 80% at (a–d) initial effective confining pressure, $\sigma_0 = 100$ kPa (~ 1 atm), and (e–h) initial effective confining pressure, $\sigma_0 = 600$ kPa (~ 6 atm).

end of shaking was much faster at 6 atm as compared to 1 atm in the centrifuge experiments. They attributed this faster dissipation of excess pore pressure at higher overburden pressure to the increased constrained modulus, M' as well as the coefficient of consolidation, C_v at 6 atm for the sand skeleton as compared to 1 atm. Abdoun et al. analytically proved that M' and C_v are approximately proportional to the square root of overburden pressure. This square root rule is the same rule inherently adopted by FLAC3D for calculating the shear modulus, G and the bulk modulus, G used to calculate the coefficient of diffusivity G from

Biot [30]. Biot's C is analogus to C_v from the classical Theory of Consolidation by Terzaghi [31] (see also [21,25] for more details).

6. Partially drained stress-controlled soil column simulations and comparison with centrifuge experiments

Again, two types of stress-controlled simulations were utilized in this research. The first is the simulation of $\underline{undrained}$ stress-controlled CDSS, presented in a previous section. The other is a simulation of $\underline{partially}$

 Table 2

 Centrifuge experiments and corresponding numerical simulations.

Experiment	Effective overburden pressure, σ'_{v0} (atm) ^a	Relative Density, D _r (%)	Numerical FLAC3D Simulation -Actual recorded acceleration input-	Numerical FLAC3D Simulation -stepped acceleration input-
Test 45-1	1	45	FLAC 45-1	FLAC 45-1 ST
Test 45-6	6	45	FLAC 45-6	FLAC 45-6 ST

^a Effective overburden pressure before shaking at mid depth of sand layer.

<u>drained</u> stress-controlled test consistent with possible field drainage scenarios. While the undrained CDSS type of simulations is commonly used by numerical modelers, the partially drained stress-controlled tests -proposed herein-is more complex and has not been given much attention. The concept of the proposed approach is explained below with the help of Fig. 10. The approach was first validated by running a stress-controlled test on an element within the soil column having the same drainage boundary conditions of the centrifuge experiments already discussed in the previous section, with the results discussed at the end of this section with the help of Fig. 11. The next section explores the approach more generally for the cases of various drainage boundaries sketched in Fig. 10.

The following features were implemented in the partially drained stress-controlled simulations (Fig. 10).

- Several 8-nodes brick zones were used and stacked on top of each other.
- The stack of zones forms a soil column connected at the nodes.
- A shear beam behavior was achieved by connecting each node to the three other nodes on the same level so that they move together.
- The initial geostatic stresses in the soil were established by running an initial analysis using the Mohr-Coulomb soil model.
- After that, the dynamic phase started in which the soil column was fixed at the base and was free elsewhere. The sand was assigned the P2Psand constitutive model during this phase.
- The sides of the soil column were impervious while the top and bottom were drainage boundaries.
- In the dynamic phase, the fluid was allowed to freely flow between the vertically stacked zones resulting in a one dimensional fully coupled mechanical-fluid flow analysis.
- A stepped acceleration function was applied at the bottom boundary which applies a constant acceleration to the soil column and reverses direction once the shear stresses reach some predefined level.
- The elevation at which the maximum shear stress condition was enforced corresponded to the elevation of maximum r_u in that run $(r_u = (r_u)_{max})$ which in turn depended on the type of drainage (Fig. 10). For the undrained case (Fig. 10a), this elevation of $r_u = (r_u)_{max}$ was near the top of the soil column. For the single drainage case (Fig. 10b), the elevation of $r_u = (r_u)_{max}$ was near the bottom of the soil column. For the double drainage case (Fig. 10c), the elevation of $r_u = (r_u)_{max}$ was at the midpoint of the soil column.

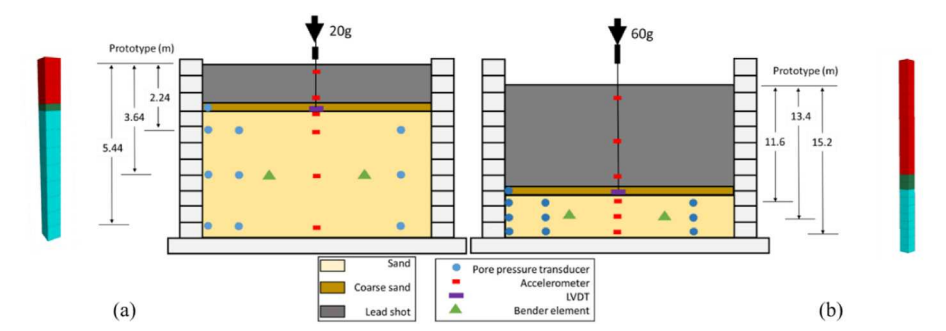


Fig. 8. Physical and numerical model layout for (a) low confining pressure test (Tests 45-1), and (b) high confining pressure test (Tests 45-6) (Ref. [25])

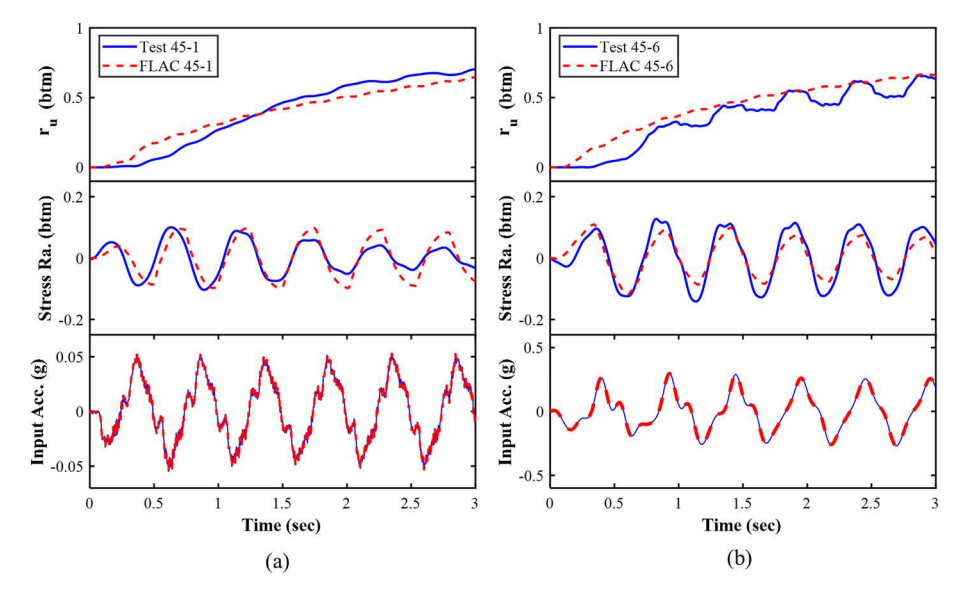


Fig. 9. Experimentally recorded and numerically computed excess pore pressure ratio histories, stress ratios, and input acceleration at the bottom of the sand layer for (a) Test 45–1, and (b) Test 45-6.

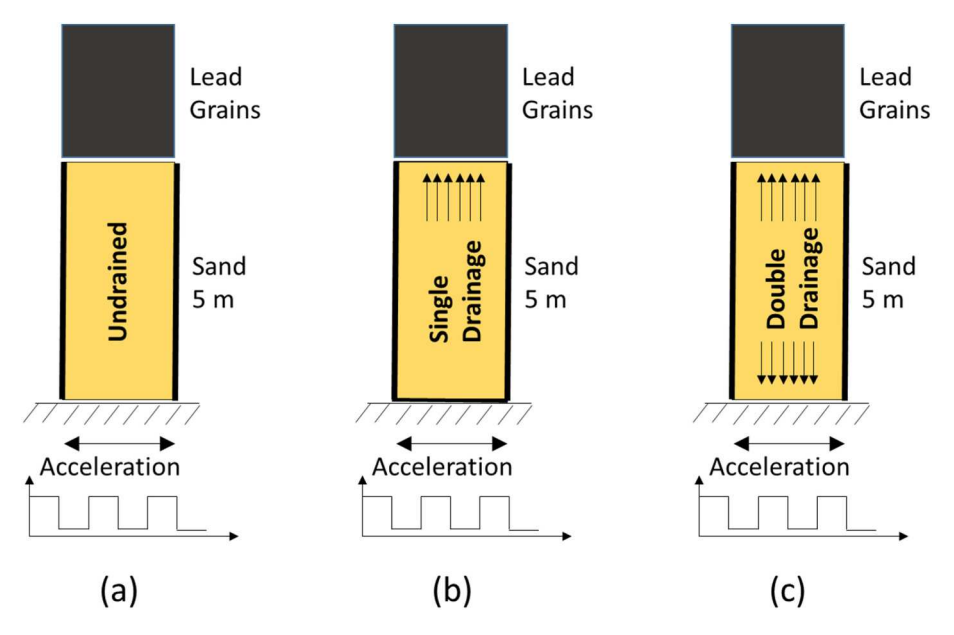


Fig. 10. (a) Undrained, (b) single drained from the top, and (c) double drained at top and bottom stress-controlled soil column numerical simulations with stepped input acceleration at the bottom.

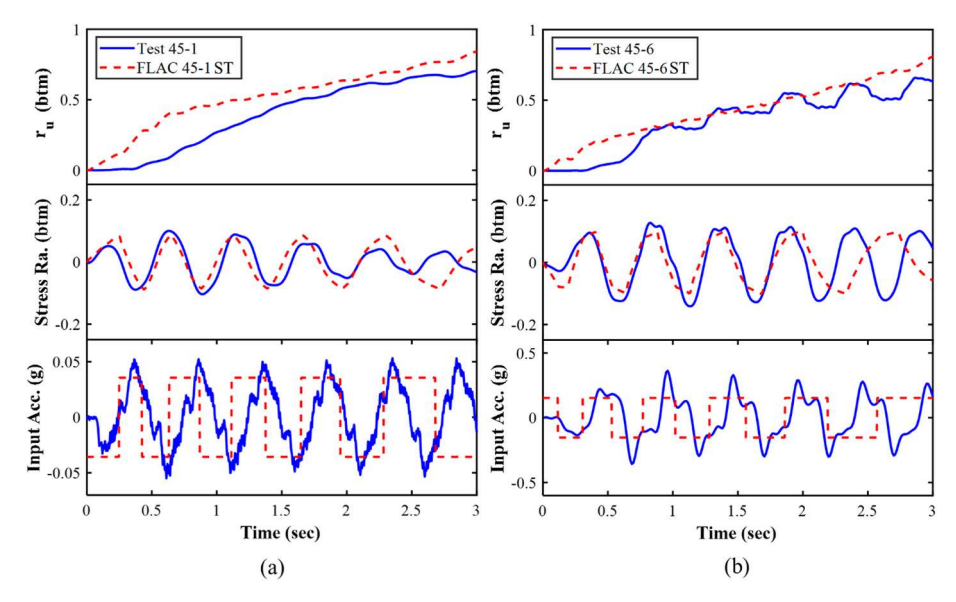


Fig. 11. Experimentally recorded and numerically computed excess pore pressure ratio histories, stress ratios, and input acceleration at the bottom of the sand layer for (a) Test 45–1 and FLAC 45-1 ST, and (b) Test 45–6 and FLAC 45-6 ST.

Applying the stepped velocity function as used in a previous section herein, is the most common method to simulate a stress controlled undrained CDSS test on a small-sample soil element. However, this method did not work with the partially drained stress-controlled tests addressed in this section, which are partially drained and are associated with a full soil column. It turns out that applying a velocity function at the base does not induce any shear stresses in the soil column, while applying it at the top mainly affects the top elevations with limited effect on the rest of the sand. The authors tried several other methods to achieve a stresscontrolled type of loading within the sand column, such as applying a constant velocity or a constant shear stress in the middle of the sand layer, but could not reach the specified goal. Also, applying a uniform sine wave input motion, such as that utilized in the centrifuge experiments, oftentimes resulted in fast pore pressure buildup and fast shear stress degradation in the sand layer at the beginning of shaking. Degraded (non-uniform) shear stress cycles yield a numerical run that is not suitable for a stress-controlled test, as it becomes challenging to select a single cyclic shear stress to represent the whole cyclic motion.

On the other hand, applying a stepped acceleration at the bottom was found to be the most acceptable and realistic methodology. It is also consistent with the actual physics of earthquake field scenarios, as well as with centrifuge modeling of these scenarios, in which accelerations are typically applied at the base of the soil column.

In order to validate this stepped acceleration approach, it was used to simulate the same centrifuge experiments discussed earlier (Tests 45–1 and 45–6). The acceleration input at the base of the soil column was adjusted to generate shear stress cycles of similar amplitude to those occurring in the centrifuge experiments, near the bottom of the sand layer, as shown in Fig. 11. Only the first 5 cycles were used in the comparison, because the experimental shear stresses degraded significantly after 5 cycles due to the excess pore pressure build up. This is not the case in the numerical simulations presented in Fig. 11 (Flac 45-1 ST

and 45-6 ST), which were meant to produce equal-amplitude shear stress cycles to simulate a partially drained stress-controlled test. Fig. 11 shows this comparison in terms of input acceleration, shear stress ratio near the bottom of the model, as well as the r_{ij} time history at the same elevation. The figure shows the difference between the shape of the actual input acceleration and the stepped input acceleration, which was adjusted to reach a similar shear stress history to that in the experiment, as shown by the shear stress ratio history comparison plots. The measured and computed r_u generally compare well. However, at the beginning of shaking the computed r_u grows much faster as compared to the recorded r_u in both plots. The reason for this deviation in behavior is that the first cycle in the experiment happened to have been smaller than the rest of acceleration cycles, so the significant rise in excess pore pressure in the experiments actually started from the second cycle. On the other hand, in the numerical simulations, all acceleration cycles had the same amplitude, so the significant rise in excess pore pressure started immediately from the beginning of shaking.

7. Effect of drainage boundaries

Fig. 10 – already discussed – presents the three drainage scenarios that were inspected herein to show the effect of pore pressure dissipation and redistribution on the liquefaction potential of sand at low and high overburden pressures (1 atm and 6 atm, respectively). The first scenario is the undrained sand in which the sand layer is assigned a very low permeability making it practically impermeable especially under short earthquake shakings. The second is the single drainage scenario in which the sand layer is assigned the same prototype permeability of the Ottawa F65 sand (0.012 m/s) used in the centrifuge experiments, while allowing the soil to drain vertically upward by assigning a free drainage boundary at the top. This was allowed in FLAC3D by assigning a very high permeability to the top overlaying layer to allow full drainage. The third case is the double drainage scenario, implemented by allowing free drainage at top and bottom. The bottom drainage was allowed numerically by maintaining a constant water pressure equal to the hydrostatic pressure at the base, thus preventing any buildup of excess pore pressure at the base of the model. A stress-controlled test was performed for each of the three scenarios of Fig. 10 using the same approach discussed in the previous section. This was repeated at both 100 kPa and 600 kPa. The specific elevation at which the maximum shear stress condition was enforced corresponded to the elevation of calculated maximum pore pressure ratio, $r_u = (r_u)_{max}$. For the top drainage condition, similar to the centrifuge experiment with the same permeability of Ottawa F65 sand, the elevation of $(r_{ij})_{max}$ was located near the bottom of the sand layer. In the undrained runs, the elevation of $(r_u)_{max}$ was near the top of the sand layer. For the double drainage condition, the elevation of $(r_u)_{max}$ was in the middle of the sand layer.

Fig. 12 shows for 1 atm, the LSCs for the three scenarios. The figure

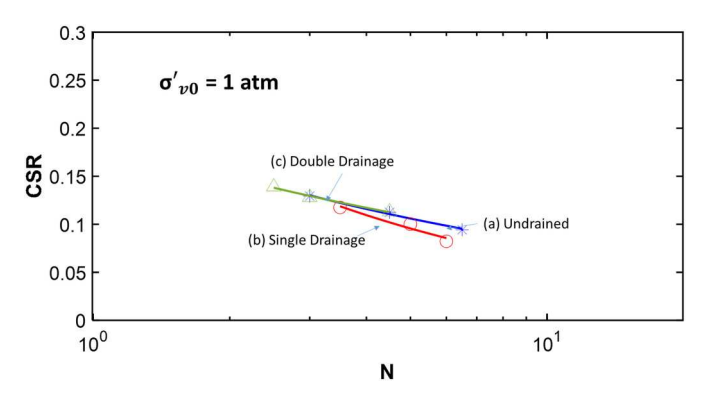


Fig. 12. LSCs of FLAC3D stress-controlled numerical simulations of partially drained soil column with average overburden pressure of about 100 kPa (1 atm) with different drainage scenarios.

shows that the LSC curves practically plot on top of each other, indicating very little effect of drainage on the liquefaction behavior of sand at relatively low (1 atm) overburden pressure.

Fig. 13 shows, respectively from the top, the shear stress ratio-strain loops, stress path (effective stresses versus shear stress ratio), excess pore pressure versus shear strain, and excess pore pressure time histories for the three drainage scenarios at 1 atm. The figure shows no significant effect of the drainage scenario on the shape of the stress-strain loops or the contraction/dilation behavior of the sand, again confirming the conclusions revealed from Fig. 12 of the almost concurrent LSCs.

Fig. 14 shows for 6 atm, the LSCs for the same three scenarios. The plot indicates that the LSC curve for the double drainage case plots the highest, indicating the least liquefaction vulnerability. The undrained LSC plots the lowest, indicating the most liquefaction vulnerability. The single drainage LSC plots in between the two extreme cases. This behavior at 6 atm contrasts with that at 1 atm, indicating a much more significant effect of drainage on the liquefaction behavior of sand at high overburden (6 atm) as compared to low overburden (1 atm).

Fig. 15 shows, for the three scenarios at 6 atm, similar plots to those in Fig. 13. The figure shows a significant effect of drainage on the dilative behavior of sand. This is especially clear from the loop reversal in the stress path (effective stresses versus shear stress ratio) which shows practically no dilative response in the undrained case. However, when one drainage boundary was added to the soil column, dilative response happened in the last cycle of shaking. When two drainage boundaries were added to the soil column, dilative behaviors happened in most shaking cycles, except for the first one or two cycles. This dilative behavior is also clear from the "Shark fin" shape of the shear stress-strain loops.

8. Summary and conclusions

Liquefaction strength curves (LSCs) are typically created by conducting undrained stress-controlled cyclic tests in order to assess the potential for liquefaction in sandy soils. However, these curves fail to account for the influence of partial drainage on liquefaction susceptibility. This limitation primarily arises from the limited experimental methods to perform stress-controlled tests on partially drained sands. This manuscript discusses the development and validation of an approach to numerically simulate a saturated sand column with a free drainage boundary at the top (or top and bottom), accelerated horizontally at the bottom with constant acceleration cycles of duration designed to generate constant cyclic shear stress histories at specified elevations within the column. This is done for columns subjected to low and high overburden pressures. The numerical work was performed using P2Psand model in FLAC3D platform. This model was calibrated by El-Sekelly et al. [25] for Ottawa F65 sand which is the cornerstone of this numerical work. The paper starts with numerical simulation of undrained CDSS by applying a stepped velocity input to a single soil element, a commonly adopted approach in numerical modeling. This approach only works for a single element which is fixed at the base and undrained. Following that, a brief description of two centrifuge tests was presented along with their corresponding numerical simulations using the same platform and model. The comparison between the experimental and numerical simulation shows a good match which gives confidence on the use of the same calibration to develop the numerical approach of partially drained stress-controlled tests. Finally, a proposed numerical approach of applying stepped acceleration at the base was used to perform partially drained stress-controlled tests at selected elevations in soil columns. This technique is used to show the effect of drainage boundaries on the liquefaction behavior at low and high overburden pressures.

Based on the numerical work presented herein, the following conclusions were reached.

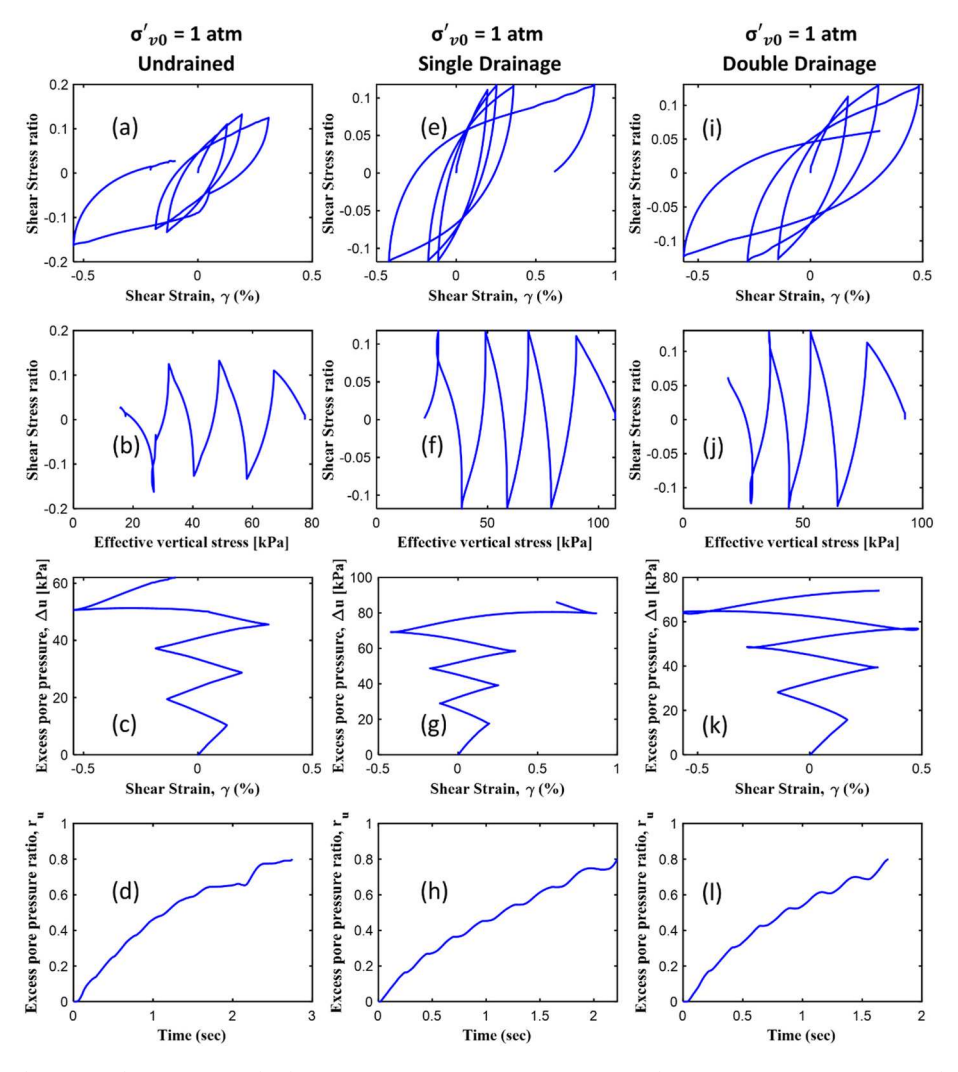


Fig. 13. Shear stress ratio-shear strain loops, stress path, shear strain versus excess pore pressure, and excess pore pressure ratio time history for stress-controlled tests of soil column with average overburden pressure of about 100 kPa (1 atm) (a–d) undrained, (e–h) single drainage from the top, and (i–l) double drainage from the top and bottom.

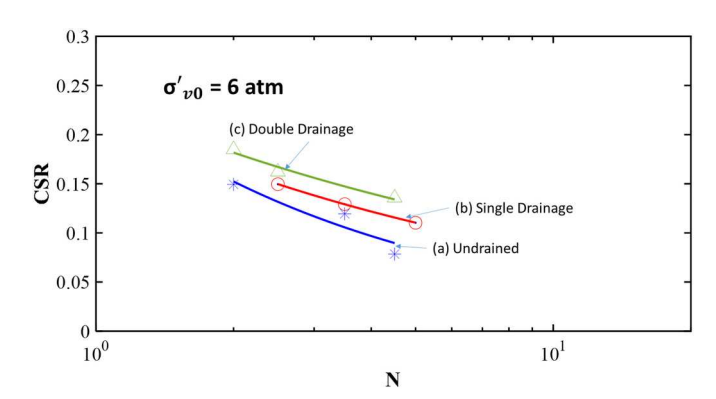


Fig. 14. LSCs of Flac3D stress-controlled numerical simulations of partially drained soil column with average overburden pressure of about 600 kPa (6 atm) with different drainage scenarios.

 A numerical approach is developed to model partially drained stresscontrolled tests in plausible field scenarios. This approach was validated based on two centrifuge experiments conducted under low and high overburden pressures with drainage allowed only at the top.
 The approach paves the road for the development of field LSCs that take partial drainage into account.

- Figs. 12 and 14 suggest that the effect of drainage is much more significant at a higher overburden stress. For a higher overburden, adding top and bottom drainage boundaries resulted in the highest LSC (i.e. less liquefaction vulnerability), compared with having only one drainage boundary on top of the sand layer.
- Based on the above conclusion, a liquefiable sand layer in the field may be less prone to liquefaction under a high overburden pressure than assumed by the current state-of-practice. This current state-ofpractice relies mainly on undrained small-scale cyclic tests and LSCs. The work herein shows that liquefaction may be a partially drained process in the field in some cases, with this partial drainage being more significant at high overburden pressures.
- While the conclusions reported herein cannot be directly generalized to all field drainage scenarios, this developed approach may easily be extended to other field conditions. Such conditions include, but are not limited to, different permeabilities, different sand thicknesses, different overburden pressures, etc.

CRediT authorship contribution statement

Waleed El-Sekelly: Conceptualization, Investigation, Methodology, Software, Validation, Writing – original draft. Ricardo Dobry: Investigation, Funding acquisition, Writing – review & editing. Tarek Abdoun: Investigation, Funding acquisition, Writing – review & editing.

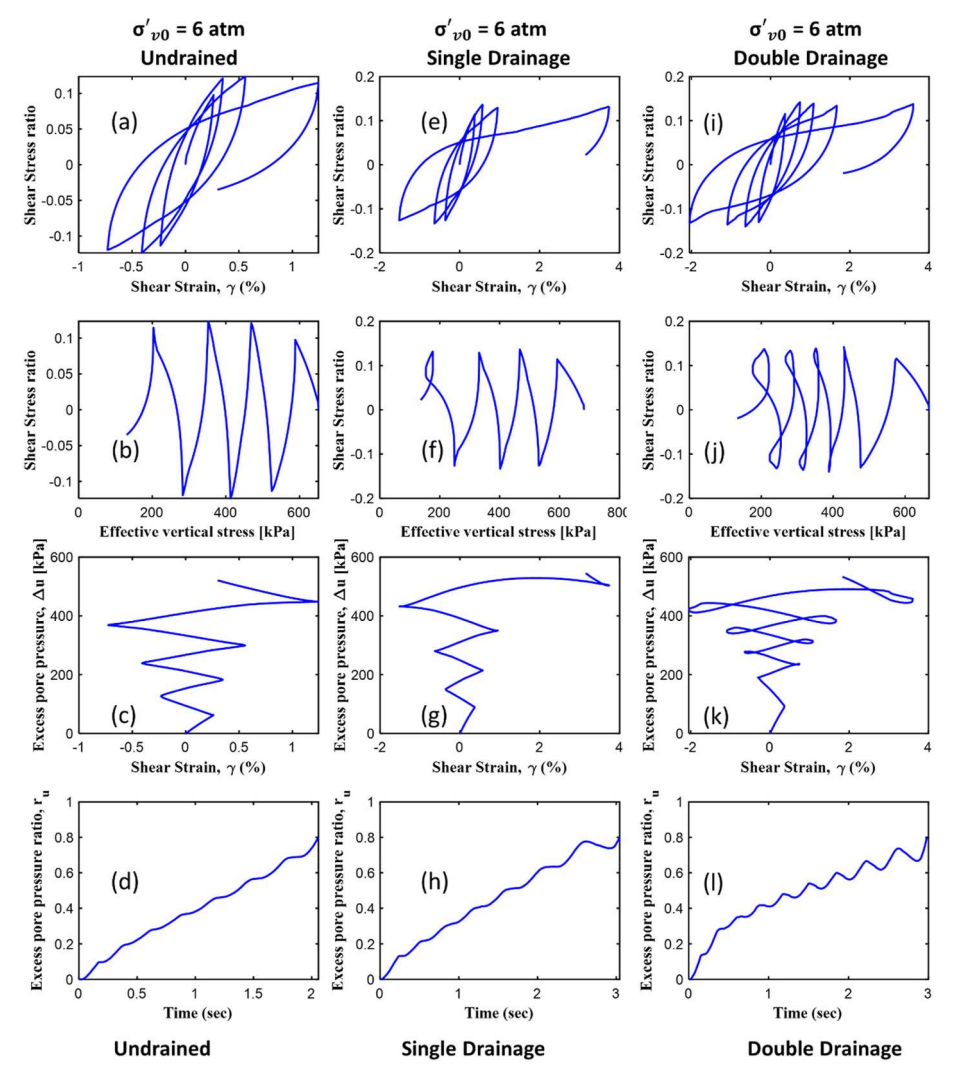


Fig. 15. Shear stress ratio-shear strain loops, stress path, shear strain versus excess pore pressure, and excess pore pressure ratio time history for stress-controlled tests of soil column with average overburden pressure of about 600 kPa (6 atm) (a–d) undrained, (e–h) single drainage at the top, and (i–l) doble drainage at top and bottom.

Declaration of competing interest

The authors declare that they have no known competing financial interests or personal relationships that could have appeared to influence the work reported in this paper.

Data availability

Data will be made available on request.

Acknowledgments

This research was performed using the FLAC3D demo version provided by Itasca Consulting Group, Inc. The authors would like to thank Dr. Zhao Cheng and Dr. Min Ni for their help throughout the course of this research. The research was supported by the National Science Foundation under Grants No. 1545026 & 1904313 and NYU Abu Dhabi; this support is gratefully acknowledged.

References

 Seed HB, Idriss IM. Simplified procedure for evaluating soil liquefaction potential. J Soil Mech Found Div 1971 Sep;97(9):1249–73.

- [2] Idriss IM, Boulanger RW. Soil liquefaction during earthquakes. Earthquake Engineering Research Institute; 2008.
- [3] De Alba PA, Chan CK, Seed HB. Sand liquefaction in large-scale simple shear tests. J Geotech Eng Div 1976 Sep;102(9):909–27.
- [4] Vaid YP, Sivathayalan S. Static and cyclic liquefaction potential of Fraser Delta sand in simple shear and triaxial tests. Can Geotech J 1996 May 8;33(2):281–9.
- [5] Seed HB. Earthquake-Resistant Design of Earth Dams. International Conferences on Recent Advances in Geotechnical Earthquake Engineering and Soil Dynamics 1981. https://scholarsmine.mst.edu/icrageesd/01icrageesd/session07/23/.
- [6] Seed RB. SPT-based analysis of cyclic pore pressure and undrained residual soil strength. In: InProc., H. Boldon Seed Memorial Symp., University of California, Berkeley. 2; 1990. p. 351–76.
- [7] Vaid YP, Thomas J. Liquefaction and postliquefaction behavior of sand. Journal of Geotechnical Engineering 1995 Feb;121(2):163–73.
- [8] Hynes ME, Olsen RS. Influence of confining stress on liquefaction resistance. Physics and mechanics of soil liquefaction 1999:145–52.
- [9] Youd TL, Idriss IM. Liquefaction resistance of soils: summary report from the 1996 NCEER and 1998 NCEER/NSF workshops on evaluation of liquefaction resistance of soils. J Geotech Geoenviron Eng 2001 Apr;127(4):297–313.
- [10] Boulanger RW. High overburden stress effects in liquefaction analyses. J Geotech Geoenviron Eng 2003 Dec;129(12):1071–82.
- [11] Boulanger RW, Idriss IM. State normalization of penetration resistance and the effect of overburden stress on liquefaction resistance. In: Proceedings 11th SDEE and 3rd ICEGE. Berkeley, CA; 2004 Jan.
- [12] Idriss IM, Boulanger RW. Semi-empirical procedures for evaluating liquefaction potential during earthquakes. Soil Dynam Earthq Eng 2006 Feb 1;26(2–4):115–30.
- [13] Montgomery J, Boulanger RW, Harder Jr LF. Examination of the K σ overburden correction factor on liquefaction resistance. Rep. No. UCD/CGM-12-02. Davis, CA: Center for Geotechnical Modeling, Dept. of Civil and Environmental Engineering, Univ. of California; 2012.

- [14] Dobry R, Abdoun T. Cyclic shear strain needed for liquefaction triggering and assessment of overburden pressure factor K σ. J Geotech Geoenviron Eng 2015 Nov 1:141(11):04015047.
- [15] Ohara S, Yamamoto T. Effect of drainage on the liquefaction resistance of saturated sand using shaking table. Soils Found 1982;22:17–22 [In Japanese)].
- [16] Umehara Y, Zen K, Hamada K. Evaluation of soil liquefaction potentials in partially drained conditions. Soils Found 1985;25:57–72.
- [17] Yamamoto Y, Hyodo M, Orense RP. Liquefaction resistance of sandy soils under partially drained condition. J Geotech Geoenviron Eng 2009;135:1032–43.
- [18] Wang B, Zen K, Chen GQ, Zhang YB, Kasama K. Excess pore pressure dissipation and solidification after liquefaction of saturated sand deposits. Soil Dynam Earthq Eng 2013;49:157–64.
- [19] Adamidis O, Madabhushi SPG. Experimental investigation of drainage during earthquake-induced liquefaction. Geotechnique 2018;68:655–65.
- [20] Chen WB, Liu K, Feng WQ, Yin JH. Partially drained cyclic behaviour of granular fill material in triaxial condition. Soil Dynam Earthq Eng 2020 Dec 1;139:106355.
- [21] Abdoun T, Ni M, Dobry R, Zehtab K, Marr A, El-Sekelly W. Pore pressure and k σ evaluation at high overburden pressure under field drainage conditions. II: additional interpretation. J Geotech Geoenviron Eng 2020 Sep 1;146(9):04020089.
- [22] Ni M, Abdoun T, Dobry R, Zehtab K, Marr A, El-Sekelly W. Pore pressure and K σ evaluation at high overburden pressure under field drainage conditions. I: centrifuge experiments. J Geotech Geoenviron Eng 2020 Sep 1;146(9):04020088.

- [23] Cheng Z, Detournay C. Formulation, validation and application of a practiceoriented two-surface plasticity sand model. Comput Geotech 2021 Apr 1;132: 103984
- [24] Dafalias YF, Manzari MT. Simple plasticity sand model accounting for fabric change effects. J Eng Mech 2004 Jun;130(6):622–34.
- [25] El-Sekelly W, Dobry R, Abdoun T, Ni M. Evaluation of field sand liquefaction including partial drainage under low and high overburden using a generalized bounding surface model. Soil Dynam Earthq Eng 2022 Jan 1;152:107059.
- [26] El Ghoraiby MA, Park H, Manzari M. LEAP-2017 GWU laboratory tests. Dataset: DesignSafe-CI; 2018.
- [27] Montgomery J, Ziotopoulou K. Numerical simulations of selected LEAP centrifuge experiments with PM4Sand in FLAC. InModel tests and numerical simulations of liquefaction and lateral spreading: LEAP-UCD-2017. Springer International Publishing; 2020. p. 481–97.
- [28] Elgamal AW, Zeghal M, Tang HT, Stepp JC. Lotung downhole array. I: evaluation of site dynamic properties. Journal of Geotechnical Engineering 1995 Apr;121(4): 350–62.
- [29] Zeghal M, Elgamal AW, Tang HT, Stepp JC. Lotung downhole array. II: evaluation of soil nonlinear properties. Journal of geotechnical engineering 1995 Apr;121(4): 363–78.
- [30] Biot MA. Theory of elasticity and consolidation for a porous anisotropic solid. J Appl Phys 1955 Feb;26(2):182–5.
- [31] Terzaghi K, Peck RB, Mesri G. Soil mechanics in engineering practice. John wiley & sons; 1996 Feb 7.